



Article

# Powder-Mixed Micro-Electro-Discharge Machining-Induced Surface Modification of Titanium Alloy for Antibacterial Properties

Nurlan Nauryz <sup>1</sup>, Salikh Omarov <sup>1</sup>, Ainur Kenessova <sup>2</sup>, Tri T. Pham <sup>2</sup> , Didier Talamona <sup>1</sup> and Asma Perveen <sup>1,\*</sup>

<sup>1</sup> Department of Mechanical & Aerospace Engineering, School of Engineering & Digital Sciences, Nazarbayev University, Astana 010000, Kazakhstan; nurlan.nauryz@alumni.nu.edu.kz (N.N.); salikh.omarov@alumni.nu.edu.kz (S.O.); didier.talamona@nu.edu.kz (D.T.)

<sup>2</sup> Department of Biology, School of Sciences and Humanities, Nazarbayev University, Astana 020000, Kazakhstan; ainur.kenessova@nu.edu.kz (A.K.); tri.pham@nu.edu.kz (T.T.P.)

\* Correspondence: asma.perveen@nu.edu.kz

**Abstract:** The powder-mixed electro-discharge machining (PM-EDM) technique has shown its advantages in forming surfaces and depositing elements on the machined surface. Moreover, using hydroxyapatite (HA) powder in PM-EDM enhances the biocompatibility of the implant's surfaces. Ti-6Al-4V alloy has tremendous advantages in biocompatibility over other metallic biomaterials in bone replacement surgeries. However, the increasing demand for orthopedical implants is leading to a more significant number of implant surgeries, increasing the number of patients with failed implants. A significant portion of implant failures are due to bacterial inflammation. Despite that, there is a lack of current research investigating the antibacterial properties of Ti-6Al-4V alloys. This paper focuses on studying the performance of HA PMEDM on Ti-6Al-4V alloy and its effects on antibacterial properties. By changing the capacitance (1 nF, 10 nF and 100 nF), gap voltage (90 V, 100 V and 110 V) and HA powder concentration (0 g/L, 5 g/L and 10 g/L), machining performance metrics such as material removal rate (MRR), overcut, crater size and hardness were examined through the HA PM micro-EDM (PM- $\mu$ -EDM) technique. Furthermore, the surface roughness, contact angle, and antibacterial properties of HA PM micro-wire EDM (PM- $\mu$ -WEDM)-treated surfaces were evaluated. The antibacterial tests were conducted for *Staphylococcus aureus*, *Pseudomonas aeruginosa*, *Escherichia coli*, and *Bacillus subtilis* bacteria. The key results showed a correlation between the discharge energy and powder concentration with the antibacterial properties of the modified surfaces. The modified surfaces exhibited reduced biofilm formation under low discharge energy and a 0 g/L powder concentration, resulting in a 0.273  $\mu$ m roughness. This pattern persisted with high discharge energy and a 10 g/L powder concentration, where the roughness measured 1.832  $\mu$ m. Therefore, it is possible to optimize the antibacterial properties of the surface through its roughness.

**Keywords:** Ti alloy; biocompatibility; antibacterial response; powder-mixed micro-EDM; surface



**Citation:** Nauryz, N.; Omarov, S.; Kenessova, A.; Pham, T.T.; Talamona, D.; Perveen, A. Powder-Mixed Micro-Electro-Discharge Machining-Induced Surface Modification of Titanium Alloy for Antibacterial Properties. *J. Manuf. Mater. Process.* **2023**, *7*, 214. <https://doi.org/10.3390/jmmp7060214>

Received: 20 October 2023

Revised: 12 November 2023

Accepted: 17 November 2023

Published: 29 November 2023



**Copyright:** © 2023 by the authors. Licensee MDPI, Basel, Switzerland. This article is an open access article distributed under the terms and conditions of the Creative Commons Attribution (CC BY) license (<https://creativecommons.org/licenses/by/4.0/>).

## 1. Introduction

Biomedical implants attract much attention in the research field due to the continuous increase in demand for bone fixing and replacement surgeries. These surgeries use metal alloys as the implanted biomaterial to repair broken bones and degenerated joints caused by injury and aging. However, these implants have a limited bio-functional response due to their artificial construction and potential complications after implantation. Along with the growing demand, this leads to an increase in the number of implant failures. One of the significant reasons for implant failure is bacterial inflammation after surgery. Although infection prevention methods can reduce the risk of surgical site infections (SSI), periprosthetic joint infection (PJI) remains a significant risk [1]. Dealing with a PJI can be tricky. According to estimates, PJIs occur in approximately 2.5% of hip and knee implant

surgeries [2], which is caused by an inability to remove bacteria from the implant surface after its first contact. In fact, if the surface of the implant is occupied by bacteria before human cells and form a bond with the surface within the first few hours, it is not possible to eliminate the infections using antibiotics or the immune system [3].

There are several existing solutions to overcome the abovementioned problem. Modifying the surface properties to repel bacteria through the surface morphology and elemental composition is a potential solution [4]. One way to achieve that is to introduce a coating on the implant material. In addition, incorporating hydroxyapatite powder during the coating process can improve the implant's ability to fight off bacteria [5–7]. Some existing techniques exist for this such as chemical vapor deposition, plasma spraying, sol-gel, physical vapor deposition, dip coating, etc. However, as most of the techniques have been known for a long time, these techniques also have some drawbacks that need to be improved. They cannot generate flawless, porous surfaces, and cannot deposit the coating and shape specimens concurrently, resulting in an increased processing cost; this is, however, possible with electro-discharge machining (EDM) [8].

EDM is a machining method with several advantages over traditional methods, including the ability to manufacture hard-to-machine materials with high precision and an excellent surface finish [9]. As shown in Figure 1, it works by using sparks between a conductive workpiece and an electrode tool [9]. Through a series of electrical discharges between the workpiece and the electrode, while using a dielectric fluid, electrical energy is converted to thermal energy in electro-discharge machining (EDM) [10]. Additionally, with the introduction of a powder additive into the dielectric fluid, EDM can be enhanced to create powder-mixed micro-EDM. The introduced powder particles decrease the breakdown strength of the dielectric gap, allowing a conductive chain to form through the gap. This in turn increases the sparking frequency, which results in faster material erosion and increases the gap between the electrode and the workpiece [11].

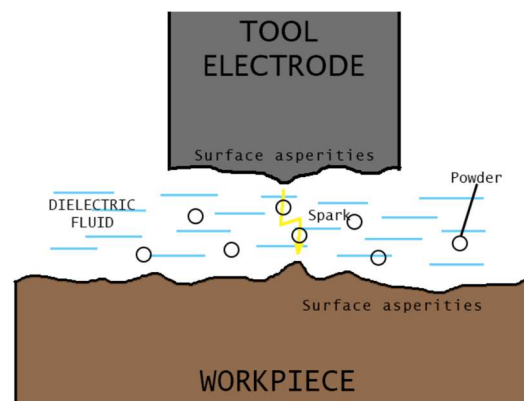


**Figure 1.** The principle of PMEDM.

Several literature reviews have explored the significant impact of a material's surface characteristics on the microstructure and cellular response in the vicinity of biomedical implants. According to the studies conducted by Kieswetter et al. and Buser et al. [12,13], the microstructure of a material plays a crucial role in influencing the accelerated development of bone or tissue around biomedical implants. Jahan et al. employed micro-EDM techniques to investigate the surface characteristics of biomedical alloys. Through micro-EDM, they examined a NiTi shape-memory alloy and high-strength Ti-6Al-4V and revealed a modification in the topography of the sample. The results showed that the NiTi had an average hardness of 420.9 HV before machining, which increased to 524.4 HV after machining, while the Ti-6Al-4V had an average hardness of 429.5 HV prior to machining and 481.6 HV following machining [14]. Additionally, regarding biological compatibility, Jahan et al. [15] reported the absence of any known harmful substances in the human body following a micro-EDM treatment of titanium alloy. Rahman et al. [16] evaluated the

surface morphology, crystallography, and chemical composition of a micro-EDM-modified surface of Ti-6Al-4V ELI. This study observed the reduction in the number of micro-pores and micro-cracks, the deposition of electrode material on the surface, and the formation of  $\alpha'$ +rutile-TiO<sub>2</sub>. The formation of chemically inert TiO<sub>2</sub> increases biocompatibility and corrosion resistance, which improves osseointegration. Along with that, there is also a formation of V<sub>2</sub>O<sub>5</sub> in the recast layer, which may cause toxic effects. Also, the dependencies of surface roughness, crater size, and recast layer thickness on peak current and pulse spacing were validated. According to Davis et al. [17], controlling the surface topography can enhance cell adhesion by obtaining the desired surface roughness. By machining Ti-6Al-4V alloy with Zn-added PM- $\mu$ -EDM, the most suitable experimental value of average surface roughness was reported to be 743.65 nm.

The choice of powder material in PMEDM significantly improves the machining performance. Different materials yield specific outcomes. For example, aluminum (Al) results in an excellent surface finish and reduced tool wear, while silicon carbide (SiC) enhances surface roughness, material removal rate, and tool wear rate [18,19]. Meanwhile, hydroxyapatite (HA) powder improves wear and corrosion resistance and provides a better biological response. However, HA is a non-conductive ceramic material [20], which makes machining less effective in terms of MRR [21]. The chemical formula for hydroxyapatite is Ca<sub>10</sub>(OH)<sub>2</sub>(PO<sub>4</sub>)<sub>6</sub>, where Ca, O, H, and P are base elements of bone. Deposition of these elements can enhance osseointegration as well [11]. Additionally, Lamichhane's study utilizing hydroxyapatite (HA) powder demonstrated an enhanced surface texture and the formation of intermetallic compounds on 316L stainless steel [22]. Further research focused on hydroxyapatite coating on titanium alloy showcased improved surface wettability, leading to enhanced cellular attachment and cell proliferation [23,24]. In terms of antibacterial properties, the effects of hydroxyapatite in PMEDM are not sufficient. Instead, some studies have investigated the antibacterial properties of HA by using other techniques, such as vacuum plasma spraying (VPS) and electrochemical deposition. From these studies, it was observed that the HA coating was able to provide antibacterial surfaces; however, some challenges still exist. During the initial stage of implantation, good antibacterial properties of the surface were achieved by introducing heavy metals and antibiotics along with HA coating. Despite that, this effect deteriorates in the long term [25]. Instead of attempts to improve the antibacterial properties of implant surfaces, much attention has been paid to silver nano-powder-mixed EDM [2,5,26]. The deposition of silver particles on the surface using the PMEDM technique significantly reduces the formation of bacteria clusters. Bui et al. [26] studied the effect of silver content on the modified surface on the biofilm formation of *S. aureus*. They found that the number of bacteria and their clusters significantly decreased up to 3.78% of silver content. However, Büsselmeier et al. [2] observed that the proliferation of bacteria remained unaffected by silver. On top of that, a significant reduction in osteoclast formation, responsible for bone resorption in its remodeling and formation, was observed. In fact, the lack of osteoclast cells allows for enhanced bone formation due to the presence of osteoblast cells [2]; however, there is a long-term importance of osteoblast cells, which contribute to the bone reforming cycle [27]. This research field is drawing increasing interest in combining silver powder's antibacterial properties and hydroxyapatite's biocompatible properties. However, many publications have used the vacuum plasma spraying (VPS) technique. Guimond et al. [5] investigated the effects of VPS-coated HA-Ag powder on titanium alloy. They concluded that the sprayed coatings provide antibacterial properties from *S. aureus* and *E. coli* to the surface, preventing cytotoxic effects on human bone cells.

Many earlier studies exploring EDM as a process for the surface modification of implants only focus on its potential as a substitute for other surface treatments. However, there is a need for a more comprehensive study that explores the effects of EDM process parameters on the generated surface and the antibacterial properties of Ti-6Al-4V alloy after EDM. Additionally, a limited number of studies have investigated the quantitative correlation between biofilm formation and EDM process parameters for the treated surface.

Moreover, it was established that hydroxyapatite coating enhanced implants' biocompatibility; however, only some studies have focused on investigating its antibacterial properties through the PMEDM process.

This research aims to address those gaps by developing a thorough understanding of the machining performance by analyzing the effects of capacitance, gap voltage, and powder concentration process parameters on MRR, overcut, crater size, and hardness response parameters with HA powder-mixed micro-EDM (HA PM- $\mu$ -EDM). Moreover, HA powder-mixed microwire EDM (HA PM- $\mu$ -WEDM) was applied to analyze surface roughness, contact angle, and attachment of bacteria such as *Staphylococcus aureus*, *Pseudomonas aeruginosa*, *Escherichia coli* and *Bacillus subtilis* on the machined surfaces.

## 2. Methodology

### 2.1. Machine and Materials

To examine how machining parameters affect Ti-6Al-4V titanium alloy, a Hybrid DT 110 Micro EDM machine with an RC-type pulse generator was utilized in this study. The chosen research material was Ti-6Al-4V alloy, which was selected due to its favorable fatigue properties in a solution-treated state and lower elastic modulus [28]. Samples of this material were cut into pieces with dimensions of 20 mm  $\times$  20 mm using a grinding method. Table 1 shows the chemical composition of this alloy. The experimental conditions and parameters are shown in Table 2.

**Table 1.** Chemical composition of Ti-6Al-4V.

Elements	Ti (wt.%)	Al (wt.%)	V (wt.%)	O (wt.%)	N (wt.%)	Si (wt.%)
Weight percentage (%)	85.35	5.34	3.7	3.04	2.49	0.08

**Table 2.** PMEDM experimental conditions and parameters.

Machine	Hybrid DT-110 $\mu$ -EDM machine
Workpiece	Material: Ti-6Al-4V Size 20 mm $\times$ 20 mm $\times$ 3 mm
Tool electrode	Material: Tungsten carbide Diameter: 680 $\mu$ m
Dielectric fluid	Hydrocarbon
Powder added to dielectric	Material: Hydroxyapatite 99.99% Average particle size: 10–15 $\mu$ m Concentrations: 0 g/L, 5 g/L, 10 g/L
Capacitance levels	1 nF, 10 nF, 100 nF
Voltage levels	90 V, 100 V, 110 V
Polarity	Negative at tool electrode

The current study observed an experimental investigation of the correlations between process and the response parameter was observed. It primarily analyzes process parameters (capacitance, voltage, powder concentration) and their impact on response parameters (MRR, overcut, hardness, crater size) using micro-EDM. Primary attention was given to the process efficiency of MRR, overcut process accuracy and surface morphology parameters, which are then correlated with bacterial attachment. However, to assess surface roughness, contact angle, and bacterial attachment on the surface, microwire EDM was employed to examine the controlled surface, which was a machined surface, and the other half was a nonmachined surface. Microwire EDM operates based on the same principles as conventional micro-EDM but uses tungsten wire as a tool instead of a tungsten rod. We used this machining technique to achieve a better visualization of the bacterial attachment

on the surface and compare the control surface with the same area of machined and un-machined surfaces.

For this research, the tool material was tungsten carbide (WC) with a 680  $\mu\text{m}$  diameter. Capacitance and voltage settings were divided into 3 levels each, which are 1 nF (1), 10 nF (2), 100 nF (3), and 90 V, 100 V, and 110 V. Every experimental trial was conducted with a 0.03 mm/min feed to machine 0.050 mm depth holes using micro-EDM machining. Sets of 9 experiments were repeated for 0, 5, and 10 g/L powder concentrations, which are also labeled as level 1, level 2, and level 3, respectively. The experimental set-up of micro-EDM is shown in Figure 2.

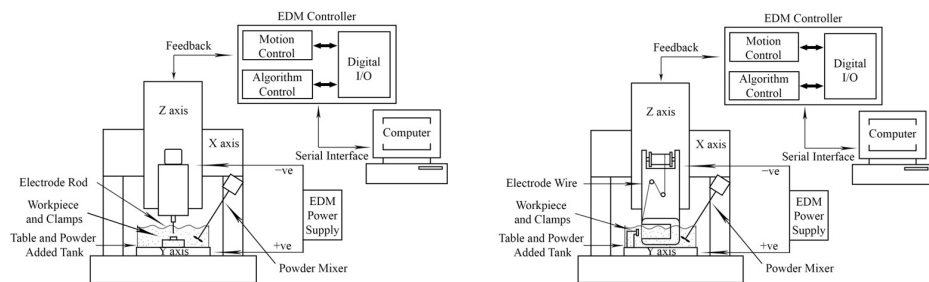


**Figure 2.** Experimental set up for micro-EDM (left) and micro-wire EDM (right) machined plates.

The powder additive was chosen to be hydroxyapatite powder, which is recognized for its durability and crystal structure. Its structure is similar to the human skeleton, making it ideal for bone implants. The dielectric fluid utilized in these experiments was hydrocarbon EDM oil.

The study investigated three process parameters: gap voltage, capacitance, and powder concentration. Taguchi array was employed in designing the set of experiments to assess the main effects among all process parameters,

A microwire EDM technique supplemented with hydroxyapatite powder was employed to assess the attachment of bacteria on Ti-6Al-4V titanium plates. Experiments were carried out by cutting a 20  $\times$  3 mm rectangle with an approximate depth of 0.025 mm on both sides of a 20  $\times$  20 mm square titanium plate using a 50  $\mu\text{m}$  diameter tungsten wire. The experimental setup for micro-WEDM machined plates is shown in Figure 2.

Given the extensive time required for each experiment (3–4 h), the number of input parameters was reduced for WEDM by dividing them into three discharge energy values: low (1 nF and 90 V), medium (10 nF and 100 V), and high (100 nF and 110 V). Each discharge energy value experiment was then repeated for two sides of the titanium plate. Furthermore, to explore the impact of hydroxyapatite powder concentration, the entire process was repeated for 0, 5, and 10 g per liter powder concentrations, resulting in six independent machined surfaces for each powder concentration.

The impact of the response parameters, including MRR, overcut, crater size, and hardness, were analyzed by estimating their SN ratios and conducting ANOVA calculations using Minitab software (19). A confidence level of 95% was chosen for the ANOVA.

## 2.2. Surface Characterization

In each trial micro-EDM, the average diameter of five craters was determined by analyzing scanning electron microscope (SEM) images. Each scanning electron microscopy (SEM) image was captured at a magnification scale 1000 $\times$ . Energy-dispersive X-ray spectroscopy (EDS) was utilized to understand the elemental composition, measuring the concentration of six elements, Ti, Al, V, C, W, and O, for each experimental condition. Surface microhardness was assessed using a Vickers microhardness tester, employing a 200-g force indenter load and 12-s dwell time. Each parameter set underwent three microhardness measurements.

We conducted experiments to examine how different input parameters for micro-WEDM impact on the surface roughness. Prior to conducting the surface roughness

measurements, the height of the probe position was calibrated using the built-in leveling indicator of the Portable Surface Roughness Gauge. During each experiment, measurements were taken on both sides of the Ti-6Al-4V plates. This approach was adopted to ensure that both sides of the plate were equally analyzed and accounted for in the final results. The Portable Surface Roughness Gauge was positioned at a fixed angle relative to the surface being measured, with the probe being moved along the surface to record the surface roughness measurements.

The contact angle measurements of Ti-6Al-4V plates were conducted using the sessile drop method with the help of OCA 25 contact angle measurement machine. These experiments were conducted on the micro-WEDM machined plates. This study chose deionized water as the liquid due to its low surface tension and excellent wettability properties.

### 2.3. Antibacterial Tests

The present study aimed to investigate the antibacterial efficacy of micro-WEDM-machined Ti-6Al-4V surfaces against various bacterial strains, namely *Staphylococcus aureus*, *Pseudomonas aeruginosa*, *Escherichia coli*, and *Bacillus subtilis*, by quantifying biofilm formation on different metal surfaces after 48 h of inoculation in broth culture. To prepare the bacterial inoculum, a fresh 24-h liquid culture of each bacterial species was used to obtain an initial optical density (OD 600) of 0.1 or a McFarland turbidity of 0.5. The OD 600 of the 24-h culture broth was measured using a microplate reader to determine the exact amount of bacteria required to add to a fresh medium in a 50 mL Falcon tube to form a final volume of 50 mL with an OD of 0.1.

Each metal alloy piece was suspended in a separate 50 mL Falcon tube containing a single bacterial species in the culture medium. These tubes were incubated under aerobic conditions in a shaker incubator at 37 °C and a speed of 220 RPM for 48 h. The metal surfaces were stained with crystal violet (CV) dye for 30 min to detect bacterial cells and biofilm formation. Afterward, the samples were rinsed three times with distilled water and left to air-dry at room temperature for 1 h before imaging. A Zeiss AxioZoom V16 microscope (Zeiss, Jena, Germany) was used to examine and capture bright-field and red fluorescent images with exposure times of 20 ms and 400 ms.

Quantitative analysis of the amount of biofilm coverage was achieved using custom-written MATLAB codes. Only biofilms with a signal greater than 200 intensity units and a size greater than five times the area of a single bacteria are collected for quantification. To ensure the cleanliness and sterilization of the metals before subsequent experiments, they were first immersed in 30% acetic acid solution for 15 min to remove any biofilms on the surfaces, then washed with autoclaved water, and finally dipped into 70% ethanol solution for 30 min, and finally plasma cleaned for 5 min. Before each biofilm formation test, all metals were sterilized under UV light for 30 min to ensure complete sterilization before culturing them with bacteria. All bacteria strains were grown in Luria–Bertani (LB) broth, with the exception of *Staphylococcus aureus*, which was grown in Tryptone Soy Broth (TSB). All experiments were conducted under aseptic conditions to prevent cross-contamination.

## 3. Results and Discussion

### 3.1. Powder-Mixed Micro-EDM

During the investigation of the effects of capacitance, voltage, and powder concentration on material removal rate (MRR) and overcut, a design of experiment (DOE) approach was used. The results indicate that both MRR and overcut were significantly affected by the levels of the factors.

Table 3 shows the values of MRR and overcut at different levels of capacitance, voltage, and powder concentration. The MRR values ranged from 8243.82 to 68,621.25  $\mu\text{m}^3/\text{s}$ , while the overcut values ranged from 9.33 to 27.00  $\mu\text{m}$ . The highest MRR value was obtained at a capacitance level of 100 nF, a voltage level of 110 V, and powder concentration level of 5 g/L. A 3D scatter plot for input variables versus MRR and overcut can be seen in Figure 3.

**Table 3.** MRR and overcut values for different levels of capacitance, voltage, and powder concentration.

Capacitance (nF)	Voltage (V)	Powder Concentration (g/L)	MRR ( $\mu\text{m}^3/\text{s}$ )	Overcut ( $\mu\text{m}$ )
1	90	0	$31,457.75 \pm 851.73$	$9.33 \pm 0.17$
1	100	5	$68,621.25 \pm 812.83$	$13.33 \pm 0.6$
1	110	10	$67,822.14 \pm 2260.38$	$13.83 \pm 0.44$
10	90	5	$8243.82 \pm 411.34$	$18.00 \pm 0.00$
10	100	10	$12,222.3 \pm 1419.19$	$18.33 \pm 0.73$
10	110	0	$15,239.51 \pm 667.97$	$16.33 \pm 0.17$
100	90	10	$44,974.1 \pm 1549.63$	$27.00 \pm 0.29$
100	100	0	$63,157.19 \pm 878.52$	$24.00 \pm 0.29$
100	110	5	$63,775.4 \pm 3023.62$	$27.00 \pm 0.50$

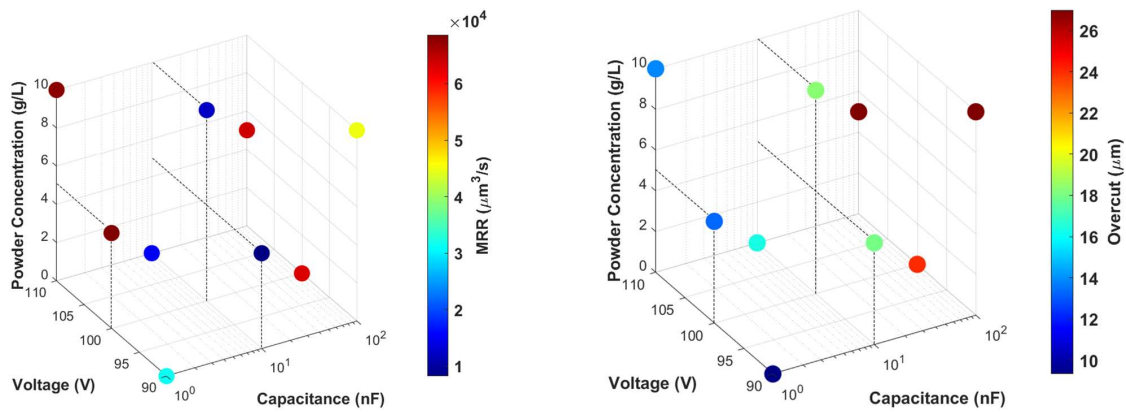


**Figure 3.** Plot showing how the MRR (left) and overcut (right) vary with different levels of capacitance, voltage, and powder concentration.

3.1.1. Material Removal Rate (MRR)

Table 4 displays the signal-to-noise ratios for the input variables, capacitance, voltage, and powder concentration, at three different levels (1, 2, and 3), with the larger signal-to-noise ratios indicating better results. It also reveals that the highest signal-to-noise ratio for MRR was obtained at level 3 (100 nF) of capacitance (95.02), followed by level 3 (110 V) of voltage (92.08), and level 2 (5 g/L of powder concentration (90.34). The rank suggests that increasing the capacitance level had the most significant effect on increasing the MRR.

**Table 4.** Response table for signal to noise ratios for material removal rate (MRR) versus capacitance, voltage, and powder concentration.

Level	Capacitance	Voltage	Powder Concentration
1	94.42	87.08	89.85
2	81.07	91.35	90.34
3	95.02	92.08	90.32
Delta	13.95	5.01	0.49
Rank	1	2	3

Increasing the capacitance and voltage settings in PMEDM results in more energy released over a specific period of time. This higher energy discharge is directed into the discharge channel, resulting in a greater material removal rate (MRR). Moreover, the addition of hydroxyapatite (HA) powder to the dielectric in PMEDM machining increases the material removal rate (MRR) due to improved electrical conductivity, enhanced heat dissipation, and formation of a bridge over the discharge gap, subsequently triggering a sequential discharge [29]. These factors facilitate efficient electrical discharges, prevent excessive temperature rise, and contribute to a higher MRR, resulting in improved machining efficiency.

Based on the delta values obtained, it can be deduced that altering the capacitance level had the most significant effect on the MRR, followed by voltage and powder concentration, with delta values of 13.95, 5.01, and 0.49, respectively. The input variables were ranked in order of importance, with capacitance being the most crucial variable for achieving high MRR values in titanium alloys' PMEDM. Therefore, if the aim is to optimize the PMEDM process parameters to achieve higher MRR values, increasing the capacitance level should be given priority.

Based on Table 5, it is evident that capacitance, voltage, and powder concentration significantly impact MRR. Their low *p*-values indicate that they are statistically significant in affecting MRR. Capacitance has the highest F-value and the lowest *p*-value among the three sources of variation, indicating that it is the most statistically significant factor for MRR. Capacitance's highest sum of squares value shows its highest contribution to MRR [30]. The impact of voltage on MRR is also significant, although to a lesser extent than that of capacitance. Even though powder concentration has the least significant effect on MRR among the three sources of variation, it is still statistically significant. Hence, all three sources of variation should be considered while optimizing the PMEDM process parameters for achieving high MRR in titanium alloys.

**Table 5.** Analysis of variance (ANOVA) table for MRR versus capacitance, voltage, and powder concentration.

Source	DF	Adj SS	Adj MS	F-Value	<i>p</i> -Value
Capacitance	2	12014140327	6007070163	183.88	0
Voltage	2	2463848020	1231924010	37.71	0
Powder concentration	2	473924286	236962143	7.25	0.004
Error	20	653369800	32668490		
Lack-of-Fit	2	524727541	262363770	36.71	0
Pure Error	18	128642259	7146792		
Total	26	15605282432			

### 3.1.2. Overcut

Table 6 shows the signal-to-noise ratios for overcut with respect to the input variables capacitance, voltage, and powder concentration. In the table, smaller values are better, as the objective is to minimize the overcut. It shows the S/N ratios for each level of the input variables and the rank based on the delta value.

**Table 6.** Response table for signal to noise ratios for overcut versus capacitance, voltage, and powder concentration.

Level	Capacitance	Voltage	Powder Concentration
1	−21.58	−24.38	−23.76
2	−24.88	−25.13	−25.42
3	−28.29	−25.24	−25.58
Delta	6.71	0.86	1.82
Rank	1	3	2

In theory, an increase in capacitance results in a drastic rise in overcut values attributed to the enhanced energy delivered during electrical discharges [31]. Similarly, an increase in voltage leads to a slight increase in overcut values due to intensified discharge energy. However, the observed increase in overcut for voltage parameter is comparatively smaller than the increase in overcut for capacitance, likely resulting from less controlled discharge behavior at higher voltages. A slightly more pronounced effect on overcut can be observed with a higher hydroxyapatite (HA) powder concentration. The reason for this is that particles in close proximity to the workpiece trigger discharges, which raises the overcut [31].

Table 6 shows that the lowest S/N ratios are obtained at level 1 for all three input variables, indicating that a lower value of capacitance, voltage, and powder concentration is beneficial for reducing the overcut. The delta values show that capacitance has the most significant effect on the overcut, followed by powder concentration and voltage. The rank order indicates that level 1 (100 nF) of capacitance is the most effective in minimizing the overcut, followed by level 3 (10 g/L) of powder concentration and level 2 (100 V) of voltage. These results suggest that reducing the capacitance, powder concentration and voltage can help to minimize the overcut during PMEDM.

The ANOVA analysis in Table 7 reveals that all three independent variables, namely capacitance, voltage, and powder concentration, significantly affect the overcut. Capacitance has the highest F-value and the lowest *p*-value, stating its most substantial statistical significance among the three variables, while the sum of squares indicates that it has the most considerable effect on the overcut.

**Table 7.** Analysis of variance (ANOVA) table for overcut versus capacitance, voltage, and powder concentration.

Source	DF	Adj SS	Adj MS	F-Value	<i>p</i> -Value
Capacitance	2	875.13	437.56	770.91	0
Voltage	2	4.019	2.00	3.54	0.048
Powder concentration	2	55.352	27.67	48.76	0
Error	20	11.352	0.56		
Lack-of-Fit	2	2.019	1.0	1.95	0.172
Pure Error	18	9.333	0.52		
Total	26	945.852			

Table 8 demonstrates the grey relational analysis (GRA) based on ANOVA. It shows that the capacitance parameter strongly influences both characteristics and performance, estimated at 83.374%. Following with lesser impact, the voltage parameter contributes around 6.182%, while the powder concentration parameter demonstrates an insignificant influence of about 1.928%.

**Table 8.** ANOVA analysis for GRA results.

Source	DF	Adj SS	Adj MS	F-Value	<i>p</i> -Value	Contribution
Capacitance	2	0.486555	0.243277	195.81	0	83.374
Voltage	2	0.036076	0.018038	14.52	0	6.182
Powder concentration	2	0.011254	0.005627	4.53	0.024	1.928
Error	20	0.024848	0.001242			
Lack-of-Fit	2	0.004118	0.002059	1.79	0.196	
Pure Error	18	0.02073	0.001152			
Total	26	0.558733				

### 3.1.3. SEM and EDS Analysis

The elemental composition of the machined holes on Ti-6Al-4V samples was investigated through SEM captures and EDS analysis after micro-EDM treatment was applied in the present study. Table 9 displays the EDS analysis before and after the treatment. The results suggest that besides the primary constituents of Ti, Al, and V, there was a material transfer from the tungsten carbide electrode and hydroxyapatite powder in the dielectric. Specifically, tungsten was found to have originated from the electrode, while the presence of calcium and phosphorus was attributed to the hydroxyapatite powder. It is worth noting that the Ti-6Al-4V alloy used in this study had a chemical composition of 85.35 wt.% Ti, 5.34 wt.% Al, 3.7 wt.% V, 3.04 wt.% O, and 2.49 wt.% C, as stated in Table 9. The chemical composition of hydroxyapatite is Ca<sub>5</sub>(PO<sub>4</sub>)<sub>3</sub>(OH). These findings suggest that the material transfer observed during micro-EDM treatment may have resulted from a combination of

electrode wear and contamination from the dielectric fluid. The EDS result of the tungsten carbide electrode shows an excessive amount of Co-Cr. It should be mentioned that Co-Cr-based biomaterials are also widely used in implant applications due to their high strength and wear resistance [32], while the inert nature of W makes it an antibacterial and biocompatible material that enhances the mechanical properties of the implant [33,34]. Some studies reported better corrosion properties when tungsten is added to the alloy (biocompatibility evaluation and corrosion resistance of tungsten-added Co-30Cr-4Mo-1Ni alloy [35]), although the pure usage of tungsten in medical implants should be avoided. The use of tungsten as a chronically implanted material has been studied [36]; however, there is no study reporting on the optimal range of tungsten usage for biocompatibility analysis. The authors of [33] reported on 27% atomic tungsten on the borosilicate substrate. The borosilicate glass coated with W-Ge exhibited notable antibiofilm properties, as evidenced by its significant reduction in the adherence of *Staphylococcus aureus* (ATCC 25923) and *Pseudomonas aeruginosa* (ATCC 27853) when compared to the control groups. In addition, the cell viability rate was reported to be 93% with respect to 21% for uncoated surfaces.

**Table 9.** Elemental analysis of Ti-6Al-4V plate before and after micro-EDM treatment.

Element	Ti	Al	V	O	C	Si	Ca	P	W	Co	Cr
Before EDM, wt.%	85.35	5.34	3.70	3.04	2.49	0.08	-	-	-	-	-
After EDM, wt.%	73.26	3.76	3.31	-	10.87	-	0.01	0.06	8.11	0.64	-
Tool, wt.%	-	-	-	21.78	6.48	-	-	-	13.34	56.91	1.49

### 3.1.4. Crater Size

This part of the study aimed to investigate the effect of input parameters, namely capacitance, voltage, and powder concentration, on the crater size during micro-EDM machining of Ti-6Al-4V using hydrocarbon dielectric. The results were analyzed by measuring the crater area for each experimental set using ImageJ software (1.53t). The data were captured in 1000× magnification in order to clearly observe the difference in crater size with the change in input parameters. Table 10 presents the crater area (μm<sup>2</sup>) values for different levels of capacitance, voltage, and powder concentration. Moreover, a 3D scatter plot of input variables versus crater size can be seen in Figure 4.

**Table 10.** Crater area values for different levels of capacitance, voltage, and powder concentration.

Capacitance (nF)	Voltage (V)	Powder Concentration (g/L)	Crater Area (μm <sup>2</sup> )
1	90	0	34.12 ± 1.99
1	100	5	42.50 ± 0.93
1	110	10	41.83 ± 2.96
10	90	5	217.31 ± 9.11
10	100	10	263.98 ± 18.08
10	110	0	317.85 ± 16.94
100	90	10	1354.61 ± 170.69
100	100	0	2111.64 ± 184.63
100	110	5	2877.31 ± 102.31

The following data were estimated using Minitab software (19). It is evident that the crater area is affected by the input parameters. For instance, according to Figures 5 and 6, with an increase in capacitance from 1 nF to 10 nF, there is a steady increase in the crater size, whereas from 10 nF to 100 nF, there is a significant increase in the crater size. This physical observation aligns with the theory that higher capacitance results in increased energy storage in the electrical discharge, leading to more intense material removal and larger crater sizes [37]. As the voltage increases, the size of the crater also increases. This is due to the higher energy that is released during discharge, which results in localized melting and vaporization of the workpiece material. The effect of powder concentration on the size of

the crater is moderate, with a slight increase from 0 g/L to 5 g/L and a gradual decrease from 5 g/L to 10 g/L. Moreover, the presence of powders can decrease surface roughness (SR) by intercepting and impeding the formation of voids in the molten metal, which would typically contribute to an increase in surface roughness during the solidification process [38]. However, in these experiments, observed effects are less pronounced due to the difficulty of maintaining a perfectly homogenous mixture of dielectric and powder additives.

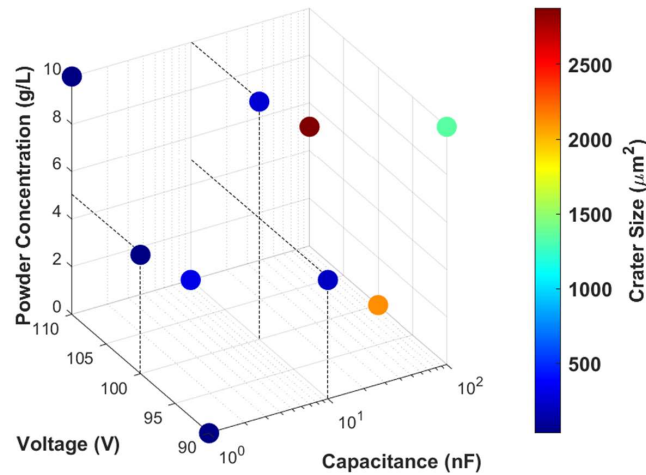


Figure 4. Plot showing how the crater size varies with different levels of capacitance, voltage, and powder concentration.

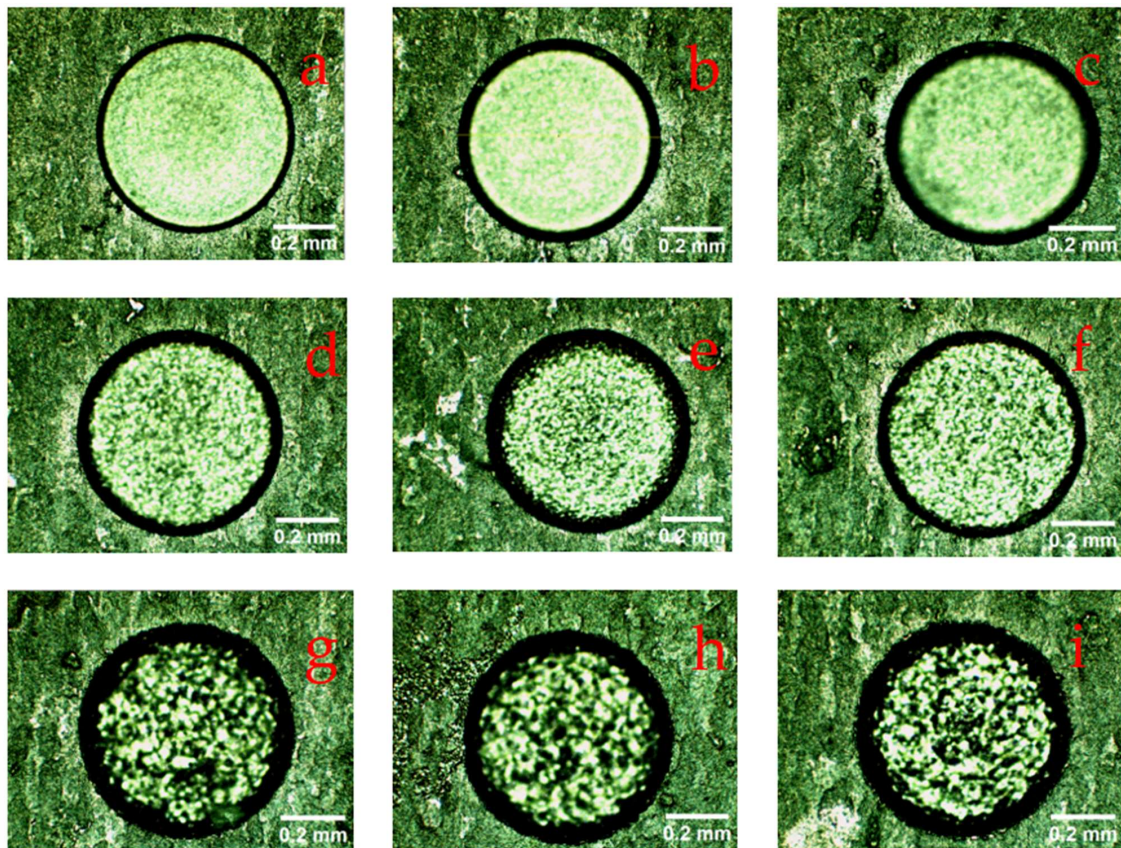
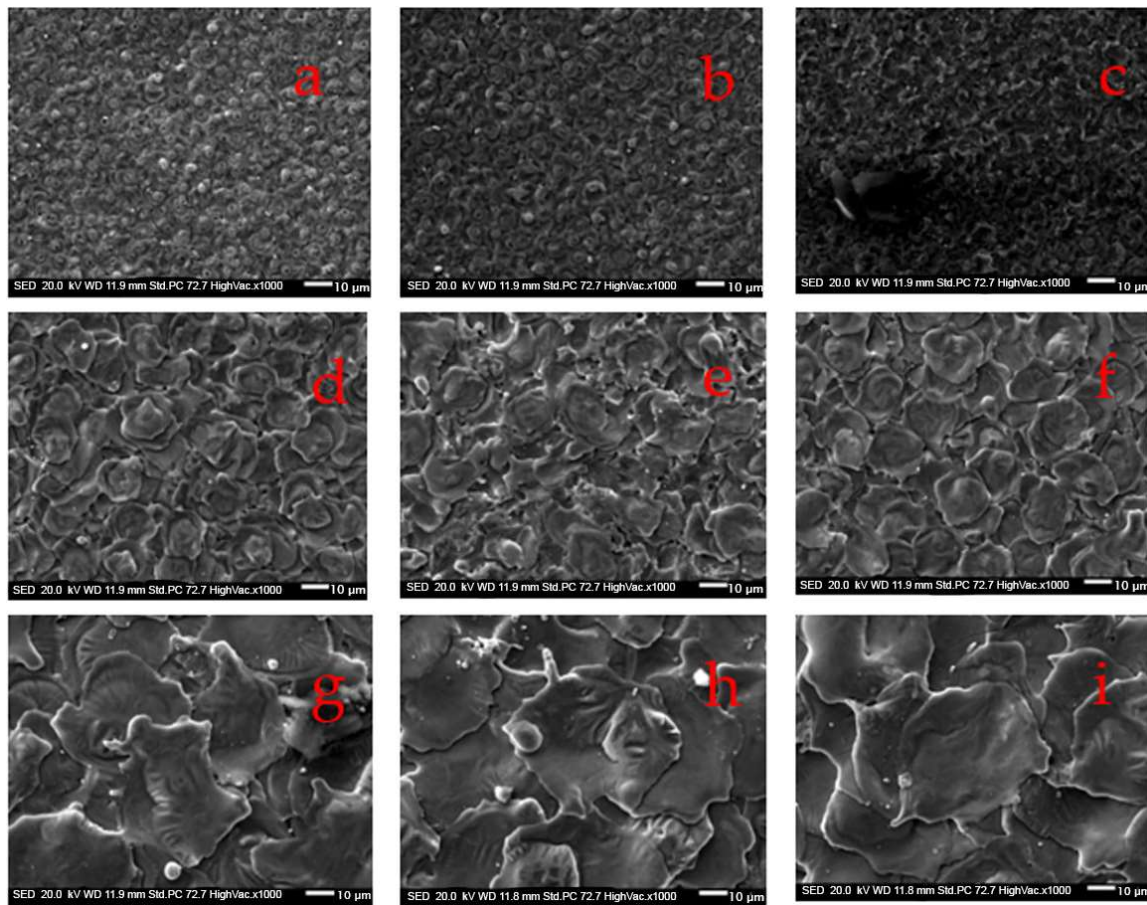


Figure 5. Optical microscope captures of micro-EDM-treated Ti-6Al-4V holes using tungsten carbide electrode tool for different discharge energies: (a) 1 nF, 90 V; (b) 1 nF, 100 V; (c) 1 nF, 110 V; (d) 10 nF, 90 V; (e) 10 nF, 100 V; (f) 10 nF, 110 V; (g) 100 nF, 90 V; (h) 100 nF, 100 V; (i) 100 nF, 110 V at constant electrode rotational speed of 1000 rpm.



**Figure 6.** SEM captures for different discharge energies for micro-EDM of Ti-6Al-4V using tungsten carbide electrode tool: (a) 1 nF, 90 V; (b) 1 nF, 100 V; (c) 1 nF, 110 V; (d) 10 nF, 90 V; (e) 10 nF, 100 V; (f) 10 nF, 110 V; (g) 100 nF, 90 V; (h) 100 nF, 100 V; (i) 100 nF, 110 V at constant electrode rotational speed of 1000 rpm.

The results were further analyzed using the signal-to-noise (SN) ratio approach. Table 11 presents the response table for SN ratios for overcut versus capacitance, voltage, and powder concentration. The delta values indicate the degree of influence of each parameter on the response, with the highest value corresponding to the most influential parameter. The results indicate that capacitance is the most influential parameter, followed by voltage and powder concentration.

**Table 11.** Response table for signal to noise ratios for crater size versus capacitance, voltage, and powder concentration.

Level	Capacitance	Voltage	Powder Concentration
1	39.48	535.35	821.2
2	266.38	806.04	1045.71
3	2114.52	1078.99	553.47
Delta	2075.04	543.65	492.24
Rank	1	2	3

The results of this study indicate that the input parameters, namely capacitance, voltage, and powder concentration, significantly impact the crater size during micro-EDM machining on Ti-6Al-4V using hydrocarbon dielectric. The findings suggest that increasing the capacitance and voltage can lead to an increase in crater size, while the effect of powder concentration is moderate.

Table 12 presents the ANOVA analysis for process parameters and their relationship with crater size results. Notably, capacitance yielded the highest F-value and the lowest *p*-value among the three parameters, signifying its significant impact on crater size. Voltage and powder concentration parameters both displayed similar results with low F-Values and relatively higher *p*-values, indicating a moderate effect on crater size measurements. An interaction plot for all parameters is available in Appendix A.

**Table 12.** ANOVA analysis for crater size results.

Source	DF	Adj SS	Adj MS	F-Value	<i>p</i> -Value
Capacitance	2	7772910	3886455	21.79	0.044
Voltage	2	443335	221667	1.24	0.446
Powder concentration	2	364381	182190	1.02	0.495
Error	2	356715	178358		
Total	8	8937340			

### 3.1.5. Hardness Test

The present study includes an analysis of the Ti-6Al-4V alloy, which has an average hardness value of 258.33 HV, serving as a baseline for comparison to the hardness values obtained from the surface on Ti-6Al-4V samples machined by micro-EDM, with and without the addition of powder.

Upon examining the data in Table 13 and Figure 7, it can be observed that hardness values obtained from the experiments varied based on the levels of capacitance, voltage, and powder concentration. The highest average hardness value was obtained at a capacitance of 100 nF, voltage of 110 V, and powder concentration of 5 g/L, followed by an average hardness value at a capacitance of 100 nF, voltage of 100 V, and a powder concentration of 0 g/L.

**Table 13.** Hardness values for all experiments.

Capacitance (nF)	Voltage (V)	Powder Concentration (g/L)	Average Hardness (HV/0.2) ± SEM
1	90	0	325.67 ± 8.65
1	100	5	336.67 ± 4.33
1	110	10	319.33 ± 9.82
10	90	5	319.67 ± 19.1
10	100	10	379.00 ± 49.24
10	110	0	356.67 ± 4.67
100	90	10	377.67 ± 6.69
100	100	0	408.00 ± 21.22
100	110	5	409.67 ± 33.24

Increasing capacitance and voltage allows for a higher energy storage in the electrical discharge. Consequently, during the discharge process, there is a greater release of energy, resulting in increased heating and melting of the material. This elevated energy dissipation can induce changes in the surface microstructure, such as phase transformations, grain refinement, or alterations in crystal structure, leading to an increase in hardness values [39].

Additionally, including powders in the dielectric material greatly improved its hardness [40]. During the PMEDM process, the heat produced can cause a molten pool formation from the dissociated elements of both the electrodes and bio-dielectric. This molten pool then sticks to the substrate after being rapidly cooled, resulting in a higher micro-hardness for the coated or recast layer [41].

Further data analysis can be conducted using Table 14 for signal-to-noise ratios. It is evident that the highest values of signal-to-noise ratios for all three factors were obtained for capacitance level 3 (100 nF), with a delta of 1.64. This finding suggests that capacitance produced the most consistent and reliable results compared to the other parameters.

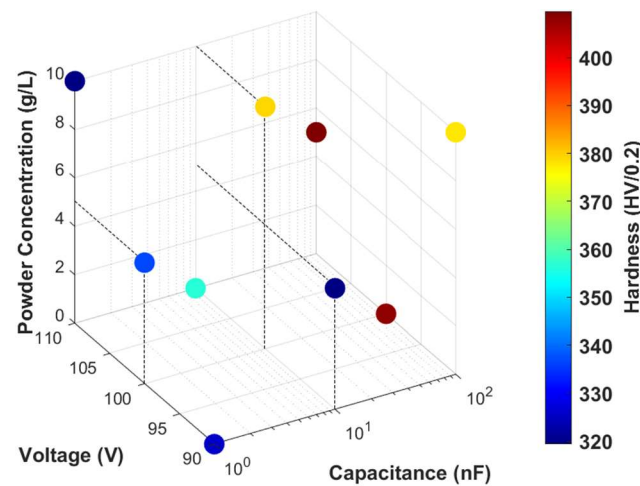


**Figure 7.** Plot showing how the hardness values varies with different levels of capacitance, voltage, and powder concentration.

**Table 14.** Response table for signal to noise ratios for surface hardness values versus capacitance, voltage, and powder concentration.

Level	Capacitance	Voltage	Powder Concentration
1	50.28	50.59	51.14
2	50.72	51.26	50.88
3	51.92	51.06	50.9
Delta	1.64	0.67	0.26
Rank	1	2	3

To conclude, the results from the Falcon 300 hardness tester for Ti-6Al-4V titanium samples machined by micro-EDM with and without powder addition demonstrate considerable variations depending on the experimental conditions employed. The highest average hardness values were observed at 100 nF capacitance, and adding powder did not always lead to an increase in hardness. It should be considered that the hardness value of hydroxyapatite is considerably smaller compared to the alloy [42,43]. Its deposition can result in a slight drop in surface hardness. Analysis of the response table for signal-to-noise ratios revealed that the powder addition had the least impact compared to other parameters, showing a delta value of 0.26. The parameter with the most significant influence on hardness increase was capacitance, with a delta value of 1.64, followed by voltage, with a delta value of 0.67. It is important to note that the present study employed tungsten carbide electrodes in micro-EDM, which may have led to the deposition of some of the carbide on the treated surface. This could potentially increase the hardness value in some of the experimental trials and adversely affect the consistency of results [41].

### 3.2. Powder-Mixed Micro-WEDM

#### 3.2.1. Surface Roughness

Surface roughness is a critical characteristic that determines the mechanical strength of materials. This study investigated the surface roughness of Ti-6Al-4V samples treated with microwire EDM by varying the input parameters. The input parameters included discharge energy and hydroxyapatite powder concentration in the hydrocarbon dielectric.

Three experiments were conducted for each combination of input parameters, and the average surface roughness values were calculated. Table 15 shows the surface roughness measurements for the microwire-EDM-treated Ti-6Al-4V workpieces.

**Table 15.** Surface roughness measurements for microwire EDM-treated Ti-6Al-4V workpieces.

Energy	Powder (g/L)	Average Roughness $\pm$ SEM ( $\mu\text{m}$ )
Low	0	$0.27 \pm 0.02$
medium	0	$0.70 \pm 0.02$
High	0	$1.68 \pm 0.06$
low	5	$0.29 \pm 0.03$
Medium	5	$0.65 \pm 0.01$
High	5	$1.77 \pm 0.05$
low	10	$0.29 \pm 0.06$
medium	10	$0.75 \pm 0.07$
High	10	$1.83 \pm 0.08$

The results indicate that the surface roughness values varied significantly depending on the input parameters. The average surface roughness values for low, medium, and high discharge energy with 0 g/L hydroxyapatite powder concentration were 0.272  $\mu\text{m}$ , 0.700  $\mu\text{m}$ , and 1.682  $\mu\text{m}$ , respectively. Similarly, for 5 g/L and 10 g/L hydroxyapatite powder concentrations, the average surface roughness values increased with the increase in discharge energy.

Furthermore, the hydroxyapatite powder concentration also affected the surface roughness values. For all three discharge energies, the average surface roughness values increased with the increase in hydroxyapatite powder concentration. For instance, at high discharge energy, the average surface roughness values were 1.682  $\mu\text{m}$ , 1.772  $\mu\text{m}$ , and 1.832  $\mu\text{m}$  for 0 g/L, 5 g/L, and 10 g/L hydroxyapatite powder concentrations.

The analysis of the provided table on surface roughness values reveals essential insights. Regardless of powder concentration, the roughness values remain relatively low at low energy levels, aligning with the expectation of less material removal and smoother surfaces. However, as the energy level increases from low to medium and then to high, there is a consistent trend of increased roughness values across all powder concentrations. This confirms that higher energy levels lead to greater material removal and surface irregularities. Furthermore, medium and high powder concentrations demonstrate a consistent pattern of increased roughness values as the energy level rises, reinforcing the notion that higher powder concentrations introduce more abrasive particles, resulting in increased material removal and surface roughness. It is imperative to consider that specific machining parameters, experimental conditions, and workpiece material characteristics can influence the exact values and potential inconsistencies in the results. Additionally, the possible inconsistencies in the measured roughness values associated with powder concentration could be attributed to an imperfect homogeneous dielectric and powder additive solution. Variations in the distribution of the powder within the solution may lead to localized concentration differences and uneven abrasion during machining, which can contribute to the observed inconsistencies in surface roughness.

### 3.2.2. Contact Angle

The contact angle of a liquid on a solid surface is a fundamental property that is influenced by various factors, including the surface roughness and the input parameters used during the treatment of the solid surface. This study measured the contact angle of Ti-6Al-4V samples treated with microwire EDM using the sessile drop method. The varied input parameters included discharge energy and hydroxyapatite powder concentration in the hydrocarbon dielectric. Three experiments were conducted for each combination of input parameters, and the average contact angle was calculated.

According to Table 16, the results exhibited that the average contact angle values varied between 45.53° and 59.57° depending on the input parameters used. Specifically, the highest average contact angle value of 59.57° was obtained for the medium energy input and a hydroxyapatite powder concentration of 10 g/L. Conversely, the lowest average

contact angle value of  $45.53^\circ$  was obtained for the low energy input and a hydroxyapatite powder concentration of 10 g/L.

**Table 16.** Surface contact angle measurements for microwire EDM-treated Ti-6Al-4V workpieces.

Energy	Powder (g/L)	Average Contact Angle $\pm$ SEM ( $^\circ$ )
Low	0	$54.67 \pm 2.04$
Medium	0	$51.5 \pm 0.19$
High	0	$54.23 \pm 0.9$
Low	5	$47.5 \pm 2.35$
Medium	5	$54.7 \pm 3.36$
High	5	$58.1 \pm 0.58$
Low	10	$45.53 \pm 0.67$
Medium	10	$59.57 \pm 1.66$
High	10	$55.27 \pm 3.14$

Interestingly, the surface roughness values also showed a notable effect on the contact angle values. The roughness values ranged from  $0.247 \mu\text{m}$  to  $1.832 \mu\text{m}$ , and a higher roughness was generally associated with a higher contact angle value. For instance, the highest surface roughness value of  $1.832 \mu\text{m}$  was obtained for the high energy input and a hydroxyapatite powder concentration of 10 g/L, which corresponded to an average contact angle of  $55.27^\circ$ . On the other hand, the lowest surface roughness value of  $0.273 \mu\text{m}$  was obtained for the low energy input and a hydroxyapatite powder concentration of 0 g/L, which corresponded to an average contact angle of  $54.67^\circ$ .

The research was focused on bacterial prevention. The measurements of contact angle assessed the hydrophilicity of EDM-machined surfaces. A contact angle below 90 degrees indicates hydrophilicity, while a greater than 90 degree contact angle signifies hydrophobicity. The consistent results showed contact angle values below 90 degrees after EDM treatment, signifying a hydrophilic surface, which is advantageous for improved biocompatibility and limited bacteria binding [44].

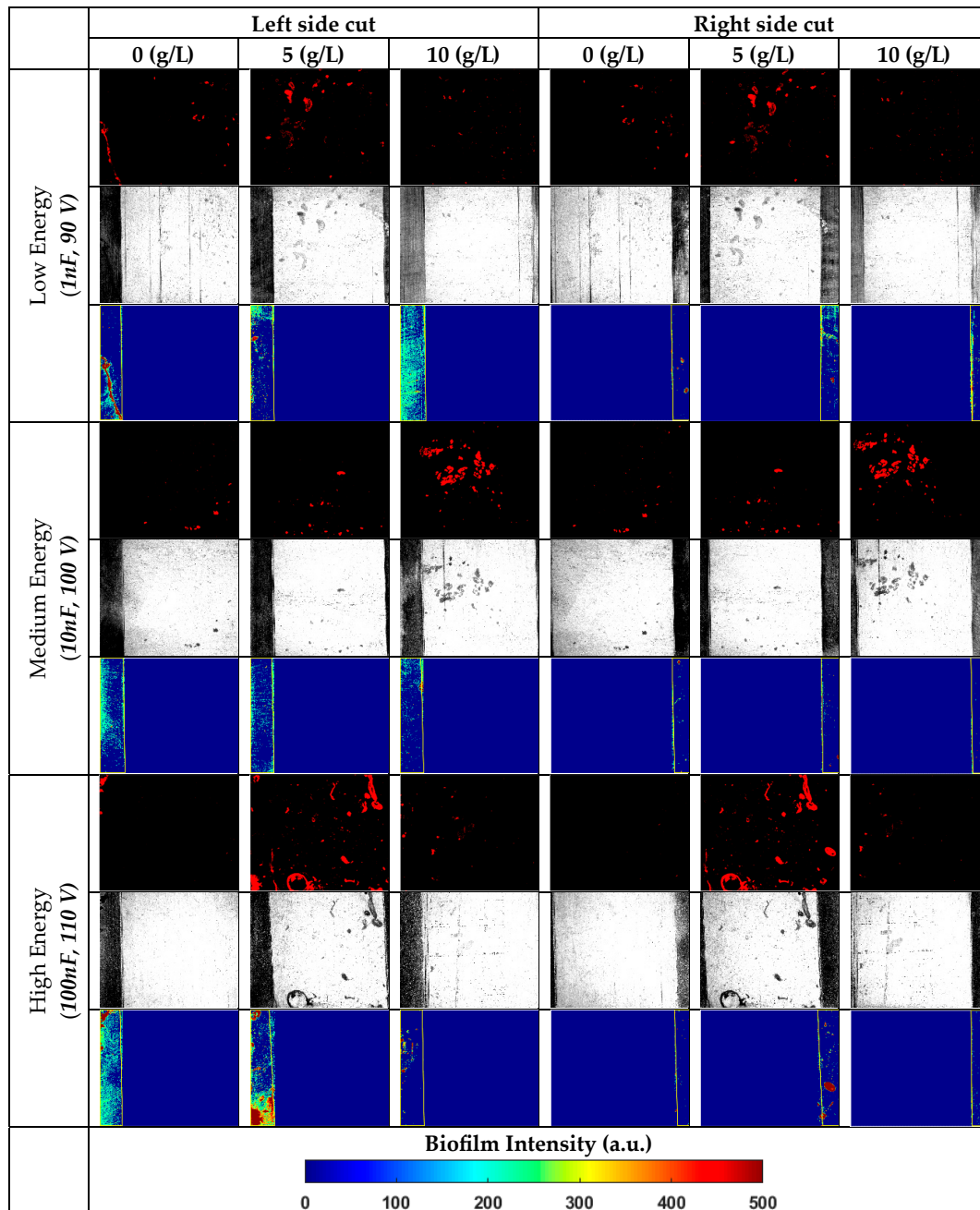
In summary, surface roughness can significantly affect the contact angle of a surface. Higher surface roughness generally corresponds to higher contact angles, indicating a more hydrophobic surface. This relationship can be attributed to the influence of surface roughness on the wetting properties of the material. Increased surface roughness creates more surface area and micro-scale features, promoting the entrapment of air or liquid within the surface irregularities. This entrapment hinders liquid spreading and leads to higher contact angles, indicating reduced wettability and a more hydrophobic surface [45].

### 3.2.3. Antibacterial Response

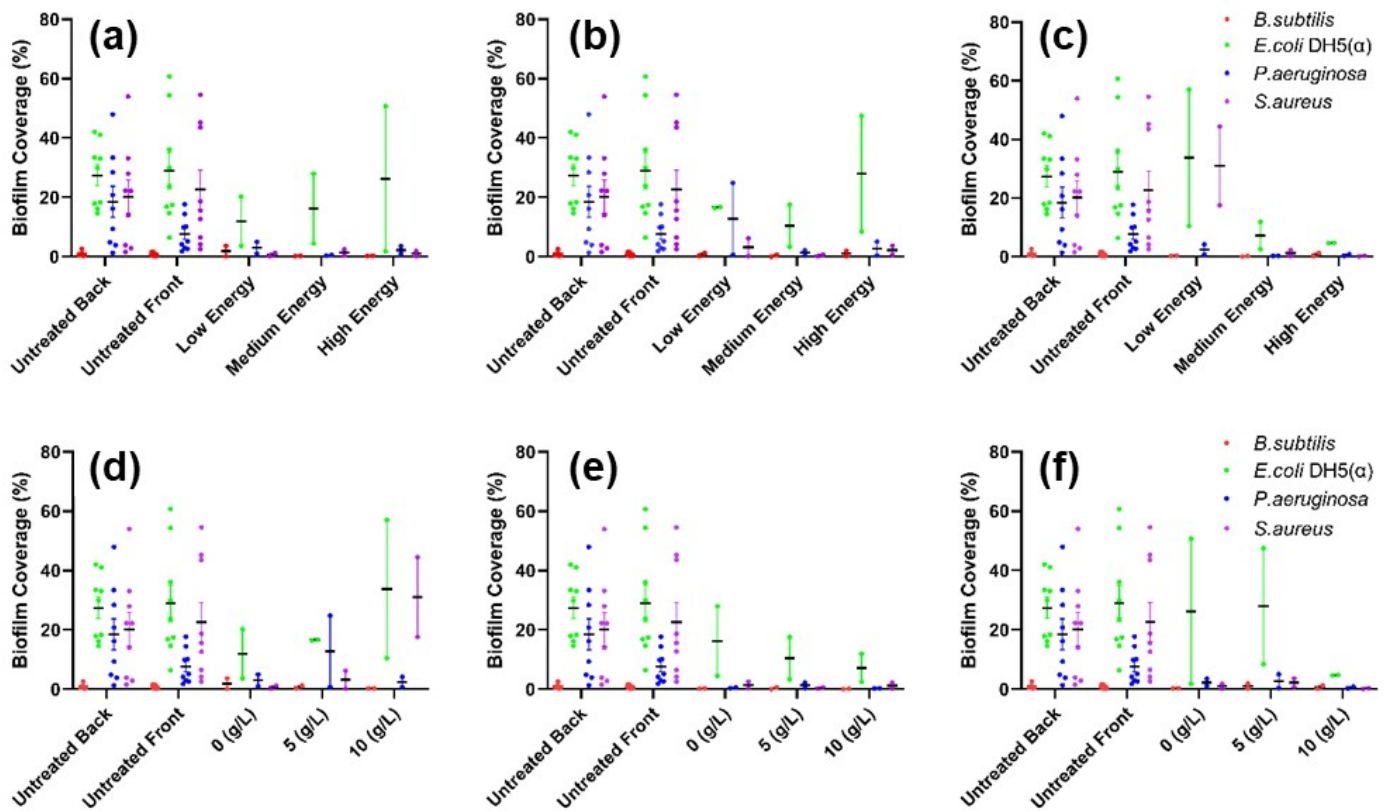
The present study aimed to investigate the effect of powder-mixed microwire EDM on the biocompatibility of Ti-6Al-4V alloy against commonly encountered bacteria strains in healthcare-associated infections, which are *Staphylococcus aureus*, *Pseudomonas aeruginosa*, and *Escherichia coli*. *Bacillus subtilis*, which is a nonpathogenic bacterial strain frequently found in soil and the gastrointestinal tracts of ruminants, humans, and marine sponges, will be used as a control. The bacterial biofilm formation was assessed using the crystal violet staining method after incubation of machined and unmachined surfaces of the Ti-6Al-4V alloy with bacteria in culture broth for 48 h.

Figure 8 depicts images of crystal violet-stained, bright field, and detected biofilm developed by *E. coli* on a micro-EDM-treated Ti-6Al-4V alloy surface at different discharge energies and powder concentrations. The effects of discharge energy level and powder concentration on the amount of biofilm formed on the alloy for all bacterial strains are shown in Figure 9. It is worth noting that *B. subtilis* does not attach to either the untreated or treated alloy surfaces, and the amount of biofilm developed is less than 2% in all conditions studied. Figure 9 also indicated that the unmachined surface of Ti-6Al-4V alloy had a higher tendency for bacterial adherence than the machined surface for the remaining three

bacterial strains. For example, Figure 9a–c clearly showed that the amount of biofilm coverage for *P. aeruginosa* and *S. aureus* significantly reduced for all applied discharge energies at 0 and 5 g/L hydroxyapatite powder concentrations. Figure 9c also shows that *S. aureus* biofilm formation increased due to low discharge energy at high powder concentrations of 10 g/L. For *E. coli*, the lowest levels of bacterial adherence were only seen at high discharge energies and high powder concentrations of 10 g/L.



**Figure 8.** Representative images of crystal violet-stained, bright field and biofilms detection for *E. coli* on machined Ti-6Al-4V alloy with different energy levels. The quantification of the percentage of biofilm coverage was performed in the machined area indicated by the yellow box on both left and right side of the alloy sample.



**Figure 9.** Quantification of biofilm coverage for all bacterial strains across all energy levels and powder concentrations. At powder concentrations of 0 g/L, 5 g/L, and 10 g/L, the effects of energy levels on biofilm coverage are shown in (a–c), respectively. The plots in (d–f) illustrate how powder concentration affects biofilm coverage at low, medium, and high energy levels.

To comprehensively investigate the effects of discharge energies and hydroxyapatite powder concentrations on biofilm development, a surface map of biofilm coverage as a function of discharge energy and hydroxyapatite powder concentration was constructed for all bacterial strains, as shown in Figure 10. It is clear that the parameters for discharge energy and powder concentration significantly influenced bacterial adherence and biofilm development on the alloy surface. These surface plots clearly show that low bacterial adhesion for all bacterial strains tested in this work may be accomplished either by utilizing low discharge energy without powder or high discharge energy with high powder concentration. The results from this study demonstrate that the strength of bacterial attachment on the machined surface of Ti-6Al-4V alloy can be tuned by adjusting the discharge energy or the concentration of hydroxyapatite powder used. Thus, producing machined alloy surfaces with antibacterial properties for any required surface roughness and crater size is entirely feasible.

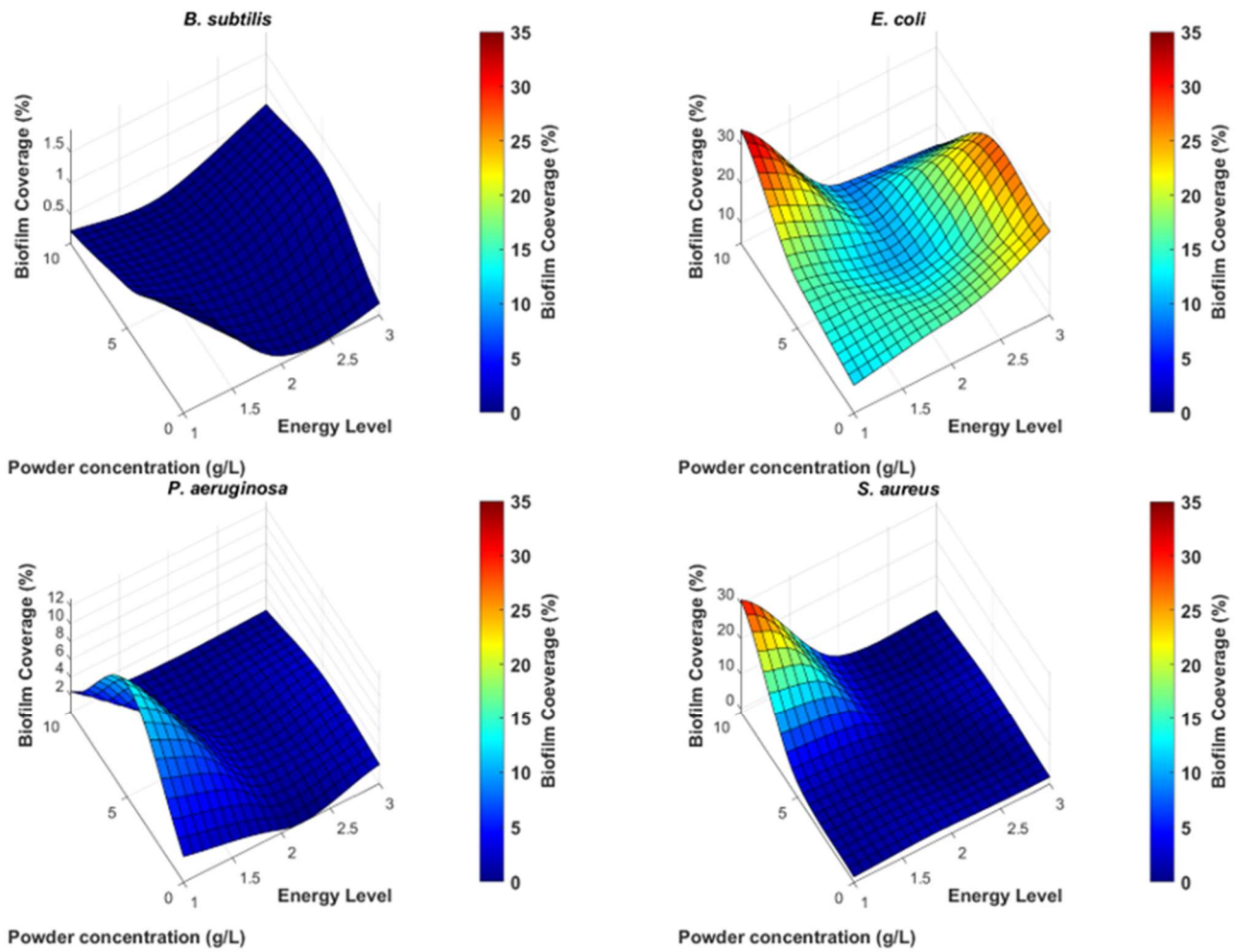


**Figure 10.** Surface plot illustrating the effects of energy level and powder concentration on the amount of biofilm that different bacterial strains can form on Ti-6Al-4V alloy after EDM treatment.

#### 4. Conclusions

In conclusion, this study aimed to enhance the antibacterial characteristics of hydroxyapatite powder-mixed micro-EDM machining on Ti-6Al-4V by gaining a comprehensive understanding of its performance. To accomplish this, a systematic investigation was conducted using micro-EDM as well as micro-WEDM techniques. Key results on antibacterial properties of machined surfaces, as well as performance parameters such as MRR, overcut, crater size, hardness, surface roughness, and contact angle, are listed below:

Optimizing capacitance, voltage, and powder concentration enhances micro-EDM machining efficiency and quality. According to tables showing the SN ratios, optimal values for MRR, overcut, crater size, and hardness were obtained. For high MRR and crater size, parameters of capacitance, gap voltage, and powder concentration were at levels 3 (100 nF), 3 (110 V), and 2 (10 g/L), respectively. For less overcut, levels of capacitance, gap voltage, and powder concentration were 1 (1 nF, 90 V, and 0 g/L, respectively). For high hardness, values of capacitance, gap voltage, and powder concentration were at levels 3 (100 nF), 2 (100 V), and 1 (0 g/L), respectively.

Performance of MRR showed that an increase in discharge energy through increasing capacitance and gap voltage affects MRR. Meanwhile, the addition of powder results in increased MRR as well.

The results of the overcut presented its dependency on the parameters. Smaller capacitance and gap voltage allow for a reduction in the sparking gap between the workpiece

and the electrode. On the contrary, the presence of powder increased the sparking distance by allowing the transfer of discharge energy through powder particles.

Crater size values showed direct dependency on the discharge energy value. Exponential changes in capacitance values resulted in corresponding changes in area values of craters. A slight influence of gap voltage was observed as well, while the contribution of powder was moderate. A total of 10 g/L powder concentration showed a sensible drop comparing to 0 g/L and 5 g/L powder concentrations. While crater size is directly affected by discharge energy, the contribution of powder to crater size can increase crater size; however, its excessive amount can result in its reduction.

The hardness values of the machined surface were increased to 319.33 HV–409.67 HV compared to the untreated Ti-6Al-4V surface, which is 258.33 HV. The increase in capacitance value shows an increase in hardness. The recast layer formed from machining is thicker after applying higher discharge energies which enhances hardness. However, the contribution of powder particles resulted in a slight drop in hardness value due to the lower hardness properties of the powder itself.

The results on surface toughness presented a clear correlation between discharge energy level and surface roughness values. As well, the higher concentration of powder increased surface roughness.

Data for contact angle showed that EDM-treated surfaces are hydrophilic, with values varied between  $45.53^\circ$  and  $59.57^\circ$ . The results showed that the value of the contact angle is smaller for smaller surface roughness. Due to the higher surface contact area resulting from increased surface roughness, the surface with a higher value of surface roughness is less hydrophilic.

Input parameters significantly influence bacterial attachment. For example, low energy, hydroxyapatite concentration, and surface roughness reduce attachment on microwire EDM-machined parts. After analyzing the results, it was discovered that *B. subtilis* only very weakly adhered to the surface of either the treated alloy or the untreated alloy, and biofilm formation remained below 2% under all experimental conditions. Low discharge energy with 0 g/L powder concentration or high discharge energy settings with high powder concentration can effectively deter bacterial adhesion on Ti-6Al-4V alloy's machined surface against all strains.

The results from SEM and EDS highlight the importance of combining different base materials and additives in order to enhance the antibacterial properties of micro-EDM-machined plates. There was also evidence of material transfer from the tungsten carbide electrode and hydroxyapatite powder, with tungsten originating from the electrode and calcium and phosphorus attributed to the hydroxyapatite powder.

In conclusion, the present study suggests that a powder-mixed microwire EDM machining technique can be an effective method to improve the biocompatibility of Ti-6Al-4V alloy against bacterial strains, particularly for high energy settings and higher hydroxyapatite powder concentrations. These findings have potential implications for the development of biomedical implants with enhanced antibacterial properties. However, further studies related to cell growth are needed to validate these results and investigate the long-term effects of the powder-mixed microwire EDM machining technique on the biocompatibility of Ti-6Al-4V alloy.

**Author Contributions:** Conceptualization, A.P. and D.T.; methodology, A.P.; software, N.N.; validation, A.P., T.T.P. and D.T.; formal analysis, N.N. and S.O.; investigation, N.N., S.O. and A.K.; resources, A.P. and T.T.P.; writing—original draft preparation, N.N., S.O., T.T.P. and A.P.; writing—review and editing, A.P. and D.T.; supervision, A.P. and D.T.; project administration, A.P.; funding acquisition, A.P. All authors have read and agreed to the published version of the manuscript.

**Funding:** This research study was funded by Nazarbayev University under the project “Multiscale Powder-Mixed EDM-Induced Functional Surfaces on Biomedical Alloys for Enhanced Mechanical, Electrochemical Corrosion, Tribological and Biological Performances” (grant No. 11022021FD2917).

**Data Availability Statement:** Data are contained within the article.

**Conflicts of Interest:** The authors declare no conflict of interest.

**Appendix A**

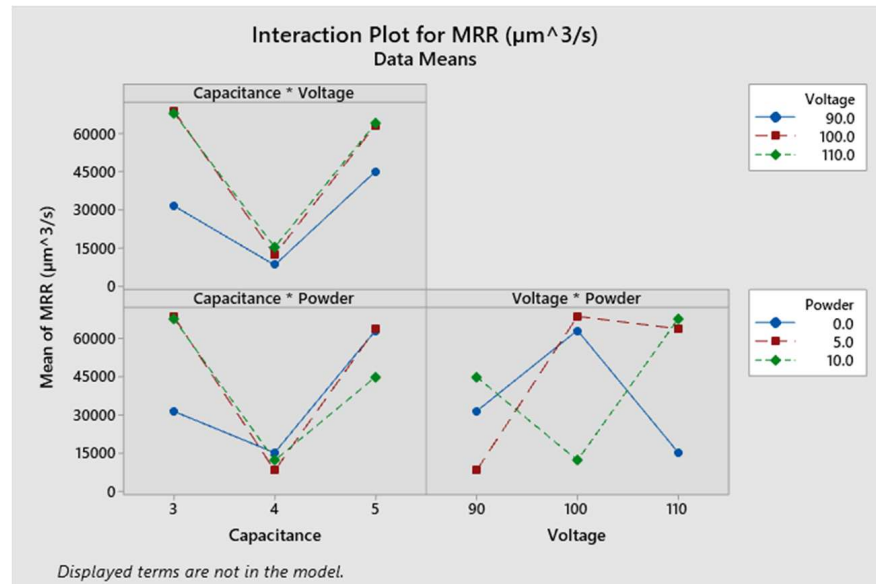


**Figure A1.** Interaction plot for MRR. \* is used for standard Inaction plot between two parameters.

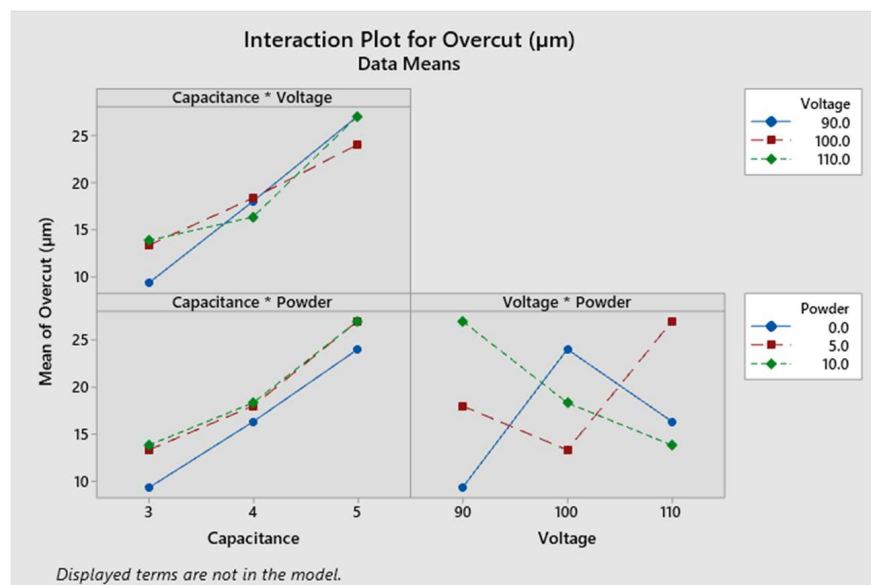


**Figure A2.** Interaction plot for overcut. \* is used for standard Inaction plot between two parameters.

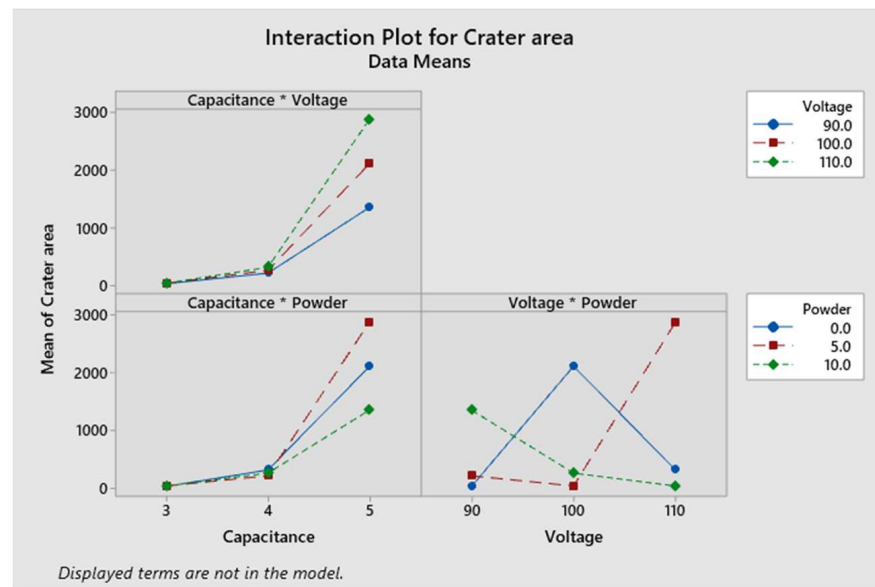


Figure A3. Interaction plot for crater size. \* is used for standard Inaction plot between two parameters.

## References

- Lentino, J.R. Prosthetic Joint Infections: Bane of Orthopedists, Challenge for Infectious Disease Specialists. *Clin. Infect. Dis.* **2003**, *36*, 1157–1161. [CrossRef]
- Büsemaker, H.; Meinshausen, A.-K.; Bui, V.D.; Döring, J.; Voropai, V.; Buchholz, A.; Mueller, A.J.; Harnisch, K.; Martin, A.; Berger, T.; et al. Silver-integrated EDM processing of TiAl6V4 implant material has antibacterial capacity while optimizing osseointegration. *Bioact. Mater.* **2024**, *31*, 497–508. [CrossRef]
- Gallo, J.; Holinka, M.; Moucha, C.S. Antibacterial Surface Treatment for Orthopaedic Implants. *Int. J. Mol. Sci.* **2014**, *15*, 13849–13880. [CrossRef]
- Nauryz, N.; Omarov, S.; Talamona, D.; Perveen, A. Performance of Powder mixed Drilling EDM on Biomedical Ti-6Al-4V Alloy. In Proceedings of the 15th International Conference on Materials Processing and Characterization (ICMPC 2023), Newcastle, UK, 5–8 September 2023; p. 01233.
- Guimond-Lischer, S.; Ren, Q.; Braissant, O.; Gruner, P.; Wampfler, B.; Maniura-Weber, K. Vacuum plasma sprayed coatings using ionic silver doped hydroxyapatite powder to prevent bacterial infection of bone implants. *Biointerphases* **2016**, *11*, 011012. [CrossRef] [PubMed]
- Ratha, I.; Datta, P.; Balla, V.K.; Nandi, S.K.; Kundu, B. Effect of doping in hydroxyapatite as coating material on biomedical implants by plasma spraying method: A review. *Ceram. Int.* **2021**, *47*, 4426–4445. [CrossRef]
- Abir, M.M.M.; Otsuka, Y.; Ohnuma, K.; Miyashita, Y. Effects of composition of hydroxyapatite/gray titania coating fabricated by suspension plasma spraying on mechanical and antibacterial properties. *J. Mech. Behav. Biomed. Mater.* **2022**, *125*, 104888. [CrossRef]
- Wang, Z.L.; Fang, Y.; Wu, P.N.; Zhao, W.S.; Cheng, K. Surface modification process by electrical discharge machining with a Ti powder green compact electrode. *J. Mater. Process. Technol.* **2002**, *129*, 139–142. [CrossRef]
- Abbas, N.M.; Solomon, D.G.; Bahari, M.F. A review on current research trends in electrical discharge machining (EDM). *Int. J. Mach. Tools Manuf.* **2007**, *47*, 1214–1228. [CrossRef]
- Kumar, S.; Singh, R.; Singh, T.P.; Sethi, B. Surface modification by electrical discharge machining: A review. *J. Mater. Process. Technol.* **2009**, *209*, 3675–3687. [CrossRef]
- Bisaria, H.; Bhusan Patra, B.; Mohanty, S. Surface modification during hydroxyapatite powder mixed electric discharge machining of metallic biomaterials: A review. *Surf. Eng.* **2022**, *38*, 680–706. [CrossRef]
- Buser, D.; Schenk, R.; Steinemann, S.; Fiorellini, J.; Fox, C.; Stich, H. Influence of surface characteristics on bone integration of titanium implants. A histomorphometric study in miniature pigs. *J. Biomed. Mater. Res. Part A* **1991**, *25*, 889–902. [CrossRef]
- Kieswetter, K.; Schwartz, Z.; Dean, D.; Boyan, B. The role of implant surface characteristics in the healing of bone. *Crit. Rev. Oral Biol. Med.* **1996**, *7*, 329–345. [CrossRef]
- Jahan, M.P.; Kakavand, P.; Alavi, F. A comparative study on micro-electro-discharge-machined surface characteristics of Ni-Ti and Ti-6Al-4V with respect to biocompatibility. *Procedia Manuf.* **2017**, *10*, 232–242. [CrossRef]
- Jahan, M.; Alavi, F.; Kirwin, R.; Mahbub, R. Micro-EDM induced surface modification of titanium alloy for biocompatibility. *Int. J. Mach. Mach. Mater.* **2018**, *20*, 274–298.

16. Rahman, S.S.; Ashraf, M.Z.I.; Bashar, M.S.; Kamruzzaman, M.; Nurul Amin, A.K.M.; Hossain, M.M. Crystallinity, surface morphology, and chemical composition of the recast layer and rutile-TiO<sub>2</sub> formation on Ti-6Al-4V ELI by wire-EDM to enhance biocompatibility. *Int. J. Adv. Manuf. Technol.* **2017**, *93*, 3285–3296. [[CrossRef](#)]
17. Davis, R.; Singh, A.; Debnath, K.; Sabino, R.M.; Papat, K.; Soares, P.; Keshri, A.K.; Borgohain, B. Enhanced Micro-Electric Discharge Machining-Induced Surface Modification on Biomedical Ti-6Al-4V Alloy. *J. Manuf. Sci. Eng.* **2022**, *14*, 071002. [[CrossRef](#)]
18. Hourmand, M.; Sarhan, A.A.; Farahany, S.; Sayuti, M. Microstructure characterization and maximization of the material removal rate in nano-powder mixed EDM of Al-Mg<sub>2</sub>Si metal matrix composite—ANFIS and RSM approaches. *Int. J. Adv. Manuf. Technol.* **2019**, *101*, 2723–2737. [[CrossRef](#)]
19. Gudur, S.; Potdar, V. Effect of silicon carbide powder mixed EDM on machining characteristics of SS 316L material experimentation. *Int. J. Innov. Res. Sci. Eng. Technol.* **2015**, *4*, 8131–8141. [[CrossRef](#)]
20. Ielo, I.; Calabrese, G.; De Luca, G.; Conoci, S. Recent Advances in Hydroxyapatite-Based Biocomposites for Bone Tissue Regeneration in Orthopedics. *Int. J. Mol. Sci.* **2022**, *2*, 9721. [[CrossRef](#)]
21. Rajamanickam, S.; Prasanna, J. Effect of Conductive, Semi-conductive and Non-conductive Powder-Mixed Media on Micro Electric Discharge Machining Performance of Ti-6Al-4V. *Int. J. Electrochem. Sci.* **2021**, *16*, 210317. [[CrossRef](#)]
22. Lamichhane, Y.; Singh, G.; Bhui, A.S.; Mukhiya, P.; Kumar, P.; Thapa, B. Surface modification of 316L SS with HAp nano-particles using PMEDM for enhanced biocompatibility. *Mater. Today Proc.* **2019**, *15*, 336–343. [[CrossRef](#)]
23. Tan, F.; O'Neill, F.; Naciri, M.; Dowling, D.; Al-Rubeai, M. Cellular and transcriptomic analysis of human mesenchymal stem cell response to plasma-activated hydroxyapatite coating. *Acta Biomater.* **2012**, *8*, 1627–1638. [[CrossRef](#)] [[PubMed](#)]
24. Bodhak, S.; Bose, S.; Bandyopadhyay, A. Role of surface charge and wettability on early stage mineralization and bone cell-materials interactions of polarized hydroxyapatite. *Acta Biomater.* **2009**, *5*, 2178–2188. [[CrossRef](#)]
25. Liao, Z.; Li, J.; Su, Y.; Miao, F.; Zhang, X.; Gu, Y.; Du, J.; Hang, R.; Wei, Y.; Chen, W. Antibacterial hydroxyapatite coatings on titanium dental implants. *Front. Mater. Sci.* **2023**, *17*, 230628. [[CrossRef](#)]
26. Bui, V.D.; Mwangi, J.W.; Meinshausen, A.-K.; Mueller, A.J.; Bertrand, J.; Schubert, A. Antibacterial coating of Ti-6Al-4V surfaces using silver nano-powder mixed electrical discharge machining. *Surf. Coat. Technol.* **2020**, *383*, 125254. [[CrossRef](#)]
27. Minkin, C.; Marinho, V.C. Role of the Osteoclast at the Bone-Implant Interface. *Adv. Dent. Res.* **1999**, *13*, 49–56. [[CrossRef](#)] [[PubMed](#)]
28. Murr, L.; Quinones, S.; Gaytan, S.; Lopez, M.; Rodela, A.; Martinez, E.; Hernandez, D.; Martinez, E.; Medina, F.; Wicker, R. Microstructure and mechanical behavior of Ti-6Al-4V produced by rapid-layer manufacturing, for biomedical applications. *J. Mech. Behav. Biomed. Mater.* **2009**, *2*, 20–32. [[CrossRef](#)] [[PubMed](#)]
29. Ou, S.-F.; Wang, C.-Y. Effects of bioceramic particles in dielectric of powder-mixed electrical discharge machining on machining and surface characteristics of titanium alloys. *J. Mater. Process. Technol.* **2017**, *245*, 70–79. [[CrossRef](#)]
30. Mohsin, I.; He, K.; Li, Z.; Zhang, F.; Du, R. Optimization of the Polishing Efficiency and Torque by Using Taguchi Method and ANOVA in Robotic Polishing. *Appl. Sci.* **2020**, *10*, 824. [[CrossRef](#)]
31. Cyril, J.; Paravasu, A.; Jerald, J.; Sumit, K.; Kanagaraj, G. Experimental investigation on performance of additive mixed dielectric during micro-electric discharge drilling on 316L stainless steel. *Mater. Manuf. Process.* **2017**, *32*, 638–644. [[CrossRef](#)]
32. Grądzka-Dahlke, M.; Dąbrowski, J.R.; Dąbrowski, B. Modification of mechanical properties of sintered implant materials on the base of Co-Cr-Mo alloy. *J. Mater. Process. Technol.* **2008**, *204*, 199–205. [[CrossRef](#)]
33. Kurt, M.S.; Arslan, M.E.; Yazici, A.; Mudu, İ.; Arslan, E. Tribological, biocompatibility, and antibiofilm properties of tungsten-germanium coating using magnetron sputtering. *J. Mater. Sci. Mater. Med.* **2021**, *32*, 6. [[CrossRef](#)]
34. Omarov, S.; Nauryz, N.; Talamona, D.; Perveen, A. Surface Modification Techniques for Metallic Biomedical Alloys: A Concise Review. *Metals* **2023**, *13*, 82. [[CrossRef](#)]
35. Aherwar, A.; Bahraminasab, M. Biocompatibility evaluation and corrosion resistance of tungsten added Co-30Cr-4Mo-1Ni alloy. *Bio-Med. Mater. Eng.* **2017**, *28*, 687–701. [[CrossRef](#)]
36. Shah Idil, A.; Donaldson, N. The use of tungsten as a chronically implanted material. *J. Neural Eng.* **2018**, *15*, 021006. [[CrossRef](#)]
37. Dewangan, S.; Kumar, S.D.; Jha, S.K.; Biswas, C.K. Optimization of Micro-EDM drilling parameters of Ti-6Al-4V alloy. *Mater. Today Proc.* **2020**, *33*, 5481–5485. [[CrossRef](#)]
38. Ekmekci, N.; Efe, Y. The effect of nano and micro hydroxyapatite powder additives on surface integrity in electrical discharge machining of Ti6Al4V alloy. *Surf. Coat. Technol.* **2022**, *445*, 128708. [[CrossRef](#)]
39. Tang, J.; Yang, X. Simulation investigation of thermal phase transformation and residual stress in single pulse EDM of Ti-6Al-4V. *J. Phys. D Appl. Phys.* **2018**, *51*, 135308. [[CrossRef](#)]
40. Prakash, C.; Kansal, H.; Pabla, B.; Puri, S. Multi-objective optimization of powder mixed electric discharge machining parameters for fabrication of biocompatible layer on β-Ti alloy using NSGA-II coupled with Taguchi based response surface methodology. *J. Mech. Sci. Technol.* **2016**, *30*, 4195–4204. [[CrossRef](#)]
41. Muthuramalingam, T.; Mohan, B.; Jothilingam, A. Effect of tool electrode resolidification on surface hardness in electrical discharge machining. *Mater. Manuf. Process.* **2014**, *29*, 1374–1380. [[CrossRef](#)]
42. Hariani, P.; Said, M.; Salni, S. Effect of sintering on the mechanical properties of hydroxyapatite from fish bone (*Pangasius Hypophthalmus*). In Proceedings of the 13th Joint Conference on Chemistry (13th JCC), Semarang, Indonesia, 7–8 September 2018; p. 012109.

43. Hervas, I.; Montagne, A.; Van Gorp, A.; Bentoumi, M.; Thuault, A.; Iost, A. Fracture toughness of glasses and hydroxyapatite: A comparative study of 7 methods by using Vickers indenter. *Ceram. Int.* **2016**, *42*, 12740–12750. [[CrossRef](#)]
44. Menzies, K.L.; Jones, L. The Impact of Contact Angle on the Biocompatibility of Biomaterials. *Optom. Vis. Sci. Off. Publ. Am. Acad. Optom.* **2010**, *87*, 387–399. [[CrossRef](#)] [[PubMed](#)]
45. Zhou, X.; De Hosson, J.T.M. Influence of surface roughness on the wetting angle. *J. Mater. Res.* **1995**, *10*, 1984–1992. [[CrossRef](#)]

**Disclaimer/Publisher’s Note:** The statements, opinions and data contained in all publications are solely those of the individual author(s) and contributor(s) and not of MDPI and/or the editor(s). MDPI and/or the editor(s) disclaim responsibility for any injury to people or property resulting from any ideas, methods, instructions or products referred to in the content.